



# Kinetics and Optimization of Azo Dye Decolorisation Using Green Synthesized Iron-Oxide Nanoparticles: A Pilot Scale Study

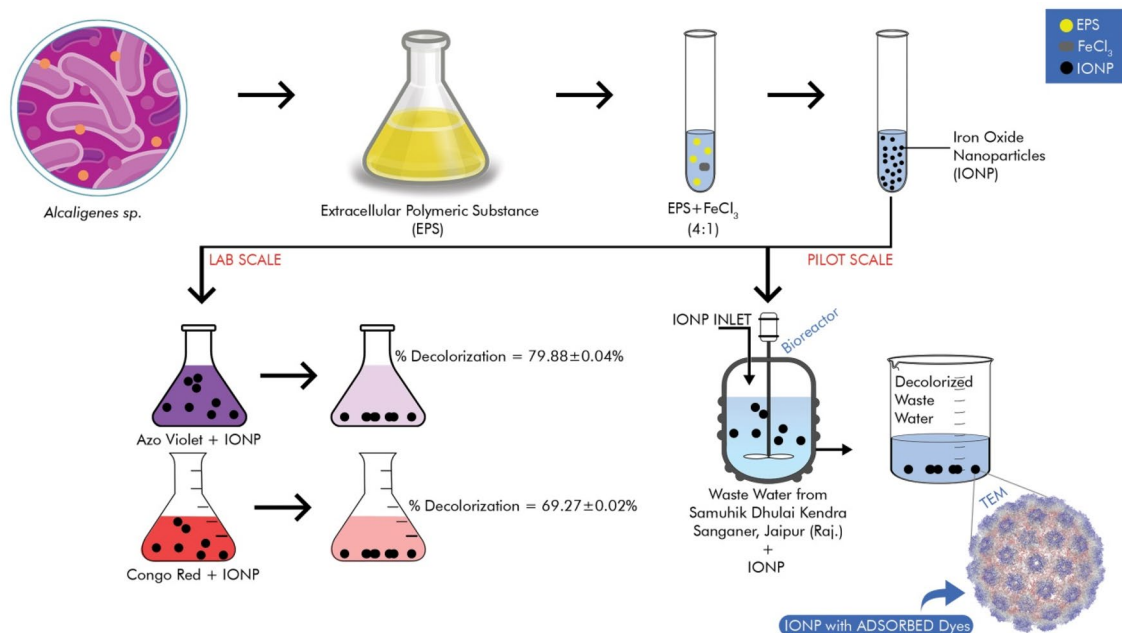
Baby Sharma<sup>1</sup> · Nilima Kumari<sup>2</sup> · Shruti Mathur<sup>1</sup> · Vinay Sharma<sup>1</sup>

Received: 3 April 2022 / Revised: 18 May 2022 / Accepted: 21 May 2022 / Published online: 15 June 2022  
© University of Tehran 2022

## Abstract

This study aims at optimizing a scalable process for decolorisation of azo dyes, using IONPs synthesized from EPS produced by the bacterium *Alcaligenes* sp. The developed process was tested for efficacy on effluents collected from washing units of Sanganer Textile Industrial Area, Rajasthan (India). The nanoparticles were characterized and tested for stability. The decolorisation process was optimized for critical parameters using Taguchi optimization method. The optimized method was then scaled up from 50 ml to a pilot scale of 2 l of effluent in the bioreactor. The mechanism of decolorisation was then evaluated. The characterization of IONPs using XRD and FTIR spectroscopy confirmed that IONPs are  $\text{Fe}_3\text{O}_4$  in nature. The IONPs were found to be stable over a period of a year with a consistent zeta potential of  $-16$  mV. Optimization using Taguchi design revealed that a concentration of 1 gm/l of dye,  $2.4 \times 10^{11}$  particles/ml of IONP, and pH 10.0 were optimum conditions for maximum decolorisation for both the dyes. Thus, at optimum conditions, a maximal decolorisation of  $79.88 \pm 0.04\%$  and  $69.27 \pm 0.02\%$  was observed for Azo Violet and Congo Red dye, respectively, with mixed order kinetics. Furthermore, scale-up of the decolorisation revealed  $81.40 \pm 0.03\%$  of decolorisation at a rate of 1.35 ml/ml IONP/min. The mechanistic study revealed aggregation pattern and size enlargement of the IONPs with change in their functional groups post-treatment which is indicative of adsorption. The above findings point to the feasibility of scalability of the process for treatment of textile industry effluents, thereby contributing to development of technologies toward circular economies.

## Graphical Abstract



## Article Highlights

- Green synthesized Iron-Oxide nanoparticles (IONPs) decolorize azo dyes.
- The IONPs are stable over a span of 1 year.
- The derived IONP based decolorisation method was found to scalable.
- Agitation remarkably improves the kinetics of the dye decolorisation.

**Keywords** Azo dyes · Nanoremediation · Iron-oxide nanoparticles · Scale-up · Green synthesized nanoparticles

## Introduction

Being the largest consumer of water, textile industries utilize voluminous water sources for various processes like dyeing and washing. It is estimated that 40–65 l of wastewater is generated while dyeing 1 kg of fabric. Most of the dyes are subsequently discharged into the environment along with waste water (Holkar et al. 2016). These untreated synthetic dyes by virtue of its recalcitrant nature are a threat to the environment. Owing to their chemical nature, these dyes are categorized into two major categories, viz., azo and non-azo dyes. Out of the two, the former is categorized more recalcitrant in nature due to the presence of azo bond (R–N=N–R') making them difficult to be degraded by natural processes (Ledakowicz and Paździor 2021).

In general, the washing after dyeing removes around 20% dyes initially used, which are mostly disposed off in the water bodies without any treatment. Such practices not only hamper the aesthetics of the water bodies but also hamper its quality by increasing excessive biological oxygen demand (BOD) and chemical oxygen demand (COD) (Yaseen and Scholz 2018). Moreover, these coloring compounds disrupt the photosynthesis by aquatic flora by hampering light penetration through water bodies (Tahir et al. 2016). This hampers every tier of the aquatic food chain. Thus, for reducing the toxicity and pollution, and for protecting the environment from the noxious impacts of dye-rich wastewaters, a number of researchers and environmentalists have emphasized on developing a variety of technologies to find out point-of-discharge treatment of the dye-rich wastewaters.

A variety of methods have been put forth for recalcitrant azo dye remediation. One such is the conventional method that involves physiochemical treatment such as membrane separation photo-degradation; adsorption; coagulation and flocculation, etc. (Dutta et al. 2021). Another method is the bioremediation method using fungi, algae, and bacteria that have been studied at lab scale (Desai et al. 2021). However, none of these methods are fit for scaling, owing to shortfalls such as mobilization of contaminant from the production site to the treatment site, microbial growth inhibition, production of sludge and issue of disposal, time-consuming, specificity for a particular dye, toxic by-products formation,

cost-ineffectiveness, etc. (Ghaly et al. 2013). In addition to this, due to economic constraints, the conventional methods of treating effluents in large-scale dyes have been proven to be ineffective. As a result of this, dye removal mediated by iron-based nanoparticles is getting increased impetus. In fact, many authors have substantiated the advantages of iron-based nanoparticles in dye bioremediation over the traditional methods (Sharma et al. 2021; Rashtbari et al. 2020). This is mainly because of its multifarious advantages such as lower toxicity, economic feasibility, high reactivity toward pollutants, quick process, and so on (Tan et al. 2015).

Being a hub of traditional textile dyeing units, Asian countries like India, Pakistan, and Bangladesh have been witnessing deterioration in local water bodies due to textile dye pollution (Yaseen and Scholz 2018). The present study encompasses an effective, proficient, and eco-friendly method for treatment of two major azo dyes used in India, viz., Azo Violet and Congo Red using green synthesized iron oxide nanoparticles (IONPs). The study also attempts to optimize the lab-scale nano-remediation process to achieve effective removal of dyes from the field samples collected from textile dyeing units of Sanganer, Rajasthan, India.

## Materials and Methods

### Materials

Iron (III) chloride [ $\text{FeCl}_3 \cdot 6\text{H}_2\text{O}$ ], mono-potassium phosphate [ $\text{KH}_2\text{PO}_4$ ], potassium phosphate dibasic [ $\text{K}_2\text{HPO}_4$ ], magnesium sulfate [ $\text{MgSO}_4 \cdot 7\text{H}_2\text{O}$ ], and calcium sulfate [ $\text{CaSO}_4 \cdot 2\text{H}_2\text{O}$ ] were purchased from Sigma-Aldrich. Yeast extract powder and sucrose were purchased from HiMedia. Two industrial grade Azo Dyes, viz., Azo Violet and Congo Red, were purchased from chemical exporter (Durga Dye Chem) of Sanganer Industrial area, Jaipur Rajasthan. Waste water was acquired from washing unit of Samuhik Dhulai Kendra, Sanganer Industrial Area, Jaipur, Rajasthan.

## Nanoparticle Synthesis and Characterization

Iron-oxide nanoparticles (IONP) were synthesized using cell-free supernatant of *Alcaligenes* sp. containing the biosurfactant and  $\text{FeCl}_3 \cdot 6\text{H}_2\text{O}$ . The method used for synthesis and characterization of nanoparticles using UV–visible spectrophotometer and TEM are represented earlier in Sharma et al. (2020). In addition to this, further characterization was done using XRD analysis which was performed to understand the crystalline structure of the synthesized IONP using Bruker d8 Advance X-ray diffractometer, using  $\text{CuK}\alpha$  radiation ( $\lambda = 1.5406 \text{ \AA}$ ), 40 kV–40 mA,  $2\theta/\theta$  scanning mode. Data were taken for the  $2\theta$  range of  $30^\circ$  to  $80^\circ$  with a step of  $0.0202^\circ$ . Apart from this, FTIR analysis was conducted with Thermoscientific FTIR with iD7 ATR Optical base for Nicolet iS5, ZnSe crystal plate for ID7 ATR and interpretation of data with software OMNIC Spectra Nicolet iS50 Edition.

## Stability of Nanoparticles

Nanoparticle stability was initially evaluated at different pH and temperature. For this, the nanoparticles were washed thrice with double-distilled water at 10,000 rpm at  $25^\circ\text{C}$  for a period 10 min each. The purified nanoparticles were re-dissolved in double-distilled water and subjected to different pH (3, 5, 7, 9, 11, 12, 13, 14) and temperature ( $10^\circ\text{C}$ ,  $25^\circ\text{C}$ ,  $50^\circ\text{C}$ ,  $80^\circ\text{C}$ ). The aqueous solutions of nanoparticles are subjected to spectrum scan in UV–visible spectrophotometer from wavelength 200 to 800 nm (Systronics119) and the peaks at absorbance maxima were evaluated.

Furthermore, to evaluate stability of IONPs with respect to time, zeta potential was evaluated using Malvern Zeta sizer (Malvern, UK). The nanoparticles were stored in aqueous medium for a period of 1 year and the zeta potential was evaluated regular interval (0 day, 6 months, and 1 year).

## Lab-Scale Dye Decolorisation Experiments

The lab-scale experiments were designed to optimize the dye remediation process using synthesized iron-based nanoparticles.

### Optimization of Critical Parameters for Decolorisation

The remediation process was subjected to initial screening to identify the suitable range of decolorisation parameters. This is done by running batch decolorisation experiments for different variables (stated in Table 1) using equal volumes of IONP and the selected azo dyes (viz., Azo Violet and Congo Red).

Prior to the remediation experiments, the concentration of the aqueous IONP solutions (as obtained in 2.3) was

**Table 1** Parameters for lab-scale optimization of decolorisation

Parameters	Range
Initial dye concentration	0.1–10 gm/l
IONP concentration	$2.4 \times 10^{11}$ – $2.4 \times 10^9$ particles/ml
pH	3–14
Temperature	$10$ – $50^\circ\text{C}$
Others	Shaking and static conditions

estimated by Hendel et al. (2014) method and diluted to different concentrations. Similarly, the dyes were dissolved in double-distilled water at varying concentrations for the remediation experiments.

To determine the decolorisation efficacy, absorbance spectra of the samples were taken using UV–Vis spectrophotometer (Systronics 119) between 200 and 800 nm. Decolorization was determined by measuring the change in absorbance of the solution at the wavelength at which maximum absorbance (432 nm for Azo Violet and 499 nm for Congo red) was obtained. An untreated dye sample was analyzed alongside as control. The percentage decolorisation is determined using Eq. 1

$$\text{Percentage decolorisation (\%)} = (A_i - A_f) \times 100/A_i, \quad (1)$$

where,  $A_i$  = initial absorbance of dye (mg/l) and  $A_f$  = final absorbance of dye (mg/l) percentage decolorisation.

### Taguchi Optimizing Method (TOM)

Experimental designs have been successfully utilized for modeling an optimal strategy for removal of a diverse range of pollutants including dyes (Süzen and Ozmetin 2019; Shokoohi et al. 2018a, b). Thus, after evaluation of the best range for each parameter and eliminating factors that had shown no significant difference, Taguchi method for optimization of the parameters was followed (Bendell et al. 1989). The method adopts the selection of most critical parameters for progression of the chemical processes. The design of the experiments was done using three different factors, viz., initial dye concentration (A), IONP concentration (B), and pH (C) which is mutually exclusive. The three parametric levels were selected, so that a reasonable range of parameter variations are included. After selecting the effective parameters in three different levels, the L-9 orthogonal array of Taguchi Optimizing Method (TOM) was used to set up the experiments (Table 2).

The Taguchi methodology employed “larger is the better” as the quality characteristic defined by Eq. 2

$$S/N_{LB} = -10 \log \frac{\sum_{i=1}^n 1/y_i^2}{n} \quad (2)$$

**Table 2** Taguchi controllable factors and their levels

Factors	Level 1	Level 2	Level 3
Initial dye concentration (gm/l)	0.1	1	1.5
IONP concentration (particles/ml)	$2.4 \times 10^{11}$	$2.4 \times 10^{10}$	$2.4 \times 10^9$
pH	11	12	13

where LB = “larger is the better”,  $n$  = number of repetitions under the same experimental conditions,  $y_i$  = measurement results.

Each experiment was repeated thrice: 1st run (R1), 2nd run (R2), and 3rd run (R3); the  $S/N$  ratio was determined using Minitab software (version 14). L and 9 mean Latin square and the number of experiments, and also, 3 and 3 indicate the numbers of factors and their levels, respectively.

The optimal parameters were identified that was involved in designing desired degradation efficiency. The maximum degradation percent is expected the desirable result.

### Kinetics of Dye Decolorisation

To determine the kinetics of IONPs for decolorisation, an initial screening was done to determine the exact time duration required for reaching the maximum decolorisation for each dye at optimal reaction conditions as determined by TOM. However, to understand the kinetics better, decolorisation was carried out at both static and shaking conditions (at 100 rpm) which were measured at varying intervals from 0 min to 1 week by measuring the absorbance at absorbance maxima in UV–Vis spectrophotometer (Systronics 119). Least square regression analysis was done to obtain the value of slopes and to determine the rate of decolorisation reaction at both static and shaking conditions.

### Scale Up to Pilot Scale

Waste water acquired from washing unit of Samuhik Dhulai Kendra, Sanganer Industrial Area, Jaipur, Rajasthan (latitude 26.797; longitude 75.6347) by random sampling method. The effluent sample was collected in sealed bottles and preserved at room temperature after filtering solid waste like cloths, threads, etc. The filtered effluent was subjected to treatment using the synthesized IONPs at optimal remediation conditions as determined above. The scale-up experiments were conducted in two phases. In the first phase of scale-up, 50 ml of purified IONP was filled in a burette and was drop-wise subjected to decolorize 50 ml of effluent sample which was placed below the burette. The reading of the IONP spent and time required for attaining maximal

visible decolorisation at optimal decolorisation condition (as obtained from 2.4) was recorded.

In the second phase, the decolorisation of 2.00 l of filtered effluent was carried out using New Brunswick BioFlo<sup>®</sup>/CelliGen<sup>®</sup> 115 bioreactor. The purified IONPs were added at a flow rate of 1.0 ml/min. The rate of agitation was 150 r.p.m. The maximal decolorisation was determined visually when there was saturation in fading of the original color. To calculate the decolorisation percentage, the pre- and post-treatment effluent samples are subjected to spectrum scan in UV–visible spectrophotometer from wavelength 200 to 800 nm (Systronics 119) and the peaks at absorbance maxima were compared.

### Mechanism of Dye Decolorisation

To understand the mechanism of the remediation process, FTIR was done for both pre- and post-treated samples from both lab-scale and pilot scale remediation studies. Moreover, morphological characterization of IONPs purified from post remediation sample of raw effluent was done using Transmission Electron Microscopy (TEM). A drop of solution was loaded on copper grids in transmission electron microscope (JEOL-2100F).

## Results and Discussion

### Nanoparticle Synthesis and Characterization

Earlier publication (Sharma et al. 2020) has reported the size of the nanoparticles as  $176.69 \pm 5.00$  nm. In the further analysis, the XRD analysis depicts highest peak intensity at a theta scale value of 27.4. The intensity count and percent intensity were found to be 159 and 100%, respectively.

The XRD pattern observed shows characteristic peaks at  $2\theta$  of 21.6, 25.77, 31.06, 40.68, 45.45, 53.49, 56.44, and 61.11 corresponding to the face-centered cubic phase of (211), (220), (202), (431), (512), (613), and (620) planes, respectively (Fig. 1). The formation of iron oxide nanoparticles in the sample was confirmed by material match analysis which revealed major presence of  $\text{Fe}_3\text{O}_4$ -NP. The obtained results from XRD are in good agreement with JCPDS card no. 019-0629. Many earlier studies have reported good agreement of iron oxide nanoparticles with the aforementioned JCPDS card no. 019-0629 (Wardani et al. 2019).

Moreover, the chemical composition as analyzed by Fourier transform infrared (FTIR) spectroscopy depicts various prominent peaks majorly at 577, 631, 991, 1631, and  $3431 \text{ cm}^{-1}$  (Fig. 1). The FTIR analysis confirms the presence iron–oxygen (Fe–O) corresponding to peaks at 577 and

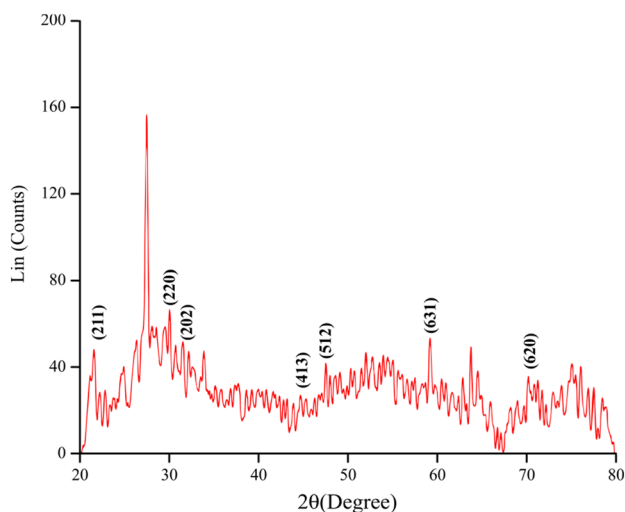


**Fig. 1** X-ray diffraction (XRD) pattern for synthesized iron oxide nanoparticle

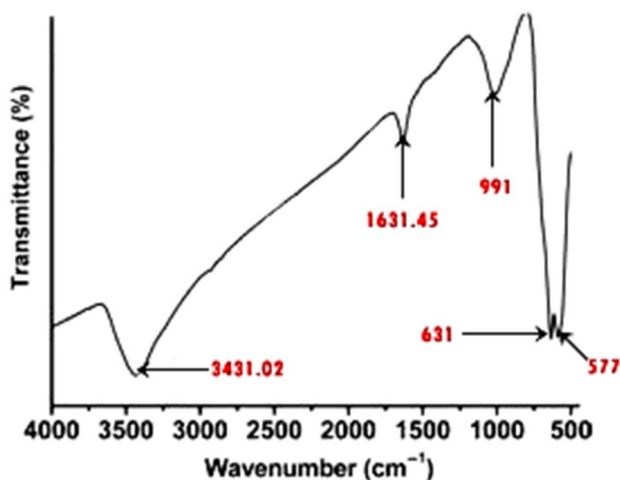


**Fig. 2** FTIR pattern for synthesized iron oxide nanoparticle

$631\text{ cm}^{-1}$ , thereby confirming the formation of iron oxide nanoparticles (Chen et al. 2013; Saharan et al. 2013). The appearance of a small peak at  $991\text{ cm}^{-1}$  is due to the presence of C–H group, the peak at  $1631\text{ cm}^{-1}$  represents bending vibration of absorbed water, and the peak at  $3431\text{ cm}^{-1}$  represents O–H stretches; hence, showing that significant impurities are extremely low (Fig. 2).

### Stability of Nanoparticles

Nanoparticle stability was evaluated at different pH and temperature, and it was observed that pH significantly affected the stability of nanoparticles (Fig. 3A), while temperature did not have any effect on the stability (Fig. 3B). The peak at absorbance maxima of the nanoparticles at  $418\text{ nm}$  was

observed at higher pH (from pH 7 onwards) owing to the stability of the nanoparticles. However, in the acidic pH, the particles were destabilized due to visible agglomeration. Similar phenomenon is reported by many earlier studies. It is in concordance with the stated fact that at higher pH, there is a higher electrostatic stability in the aqueous solution of nanoparticles due to higher surface charges creating a strong repulsive force between charged particles, thereby creating a resistance of the particles to agglomerate. Thus, alkaline condition provides an ambient condition to prevent agglomeration of nanoparticles caused by attraction and collision due to Brownian motion which is the primary reasons for destabilization of nanoparticles (Kalliola et al. 2016).

Stability of the nanoparticles remains constant over a period of 12 months. The zeta-potential values of 0 day, 6 months, and 12 months were found to be  $-16\text{ mV}$  (Fig. 4). Many authors have earlier reported negative zeta potential as an indicator of nanoparticle stability (Bhattacharjee 2016). Moreover, the negative value of zeta potential suggests a decreased particle aggregation in the continuous phase, thereby depicting its stability (Shao et al. 2015).

Many studies have earlier reported that aggregation of nanoparticles occurs during its storage (Lázár and Szabó 2018; Shrestha et al. 2020). However, the stability can be associated with the considerable presence of biosurfactants in the EPS used for the synthesis of the IONPs (as reported in earlier publication, Sharma et al. 2020). The biosurfactant acts as capping agent during the synthesis process. It improves the stability of nanoparticles (Bezza et al. 2020). Thus, the synthesized nanoparticles are stable enough to be used for the scale-up process.

### Lab-Scale Decolorisation Experiments

The lab-scale experiments were designed to optimize the dye remediation process using synthesized iron-based nanoparticles. The  $\lambda_{\text{max}}$  of both the industrial dyes that was used for evaluation of decolorisation were found to be  $432\text{ nm}$  and  $562\text{ nm}$  which is nearly concordant to the absorbance maxima of these dyes stated in the earlier studies (Rafique et al. 2021; Anouar et al. 2014).

### Optimization of Critical Parameters for Decolorisation

The initial screening experiments for the dyes gave the following results with varying reaction parameters.

**Initial Dye Concentration** Increase in initial dye concentration from  $0.1$  to  $10\text{ gm/l}$  showed that the decolorisation efficacy decreased. The maximum decolorisation of  $79.25 \pm 0.01\%$  and  $70.25 \pm 0.04\%$  was obtained from azo violet and congo red, respectively, at minimal dye concentration of  $0.1\text{ gm/l}$  (Table 3). The saturation of decol-



**Fig. 3** **A** Effect of pH on stability of IONPs. **B** Effect of temperature on stability of IONPs as observed at  $\lambda_{\text{max}} = 418$  nm of synthesized IONP

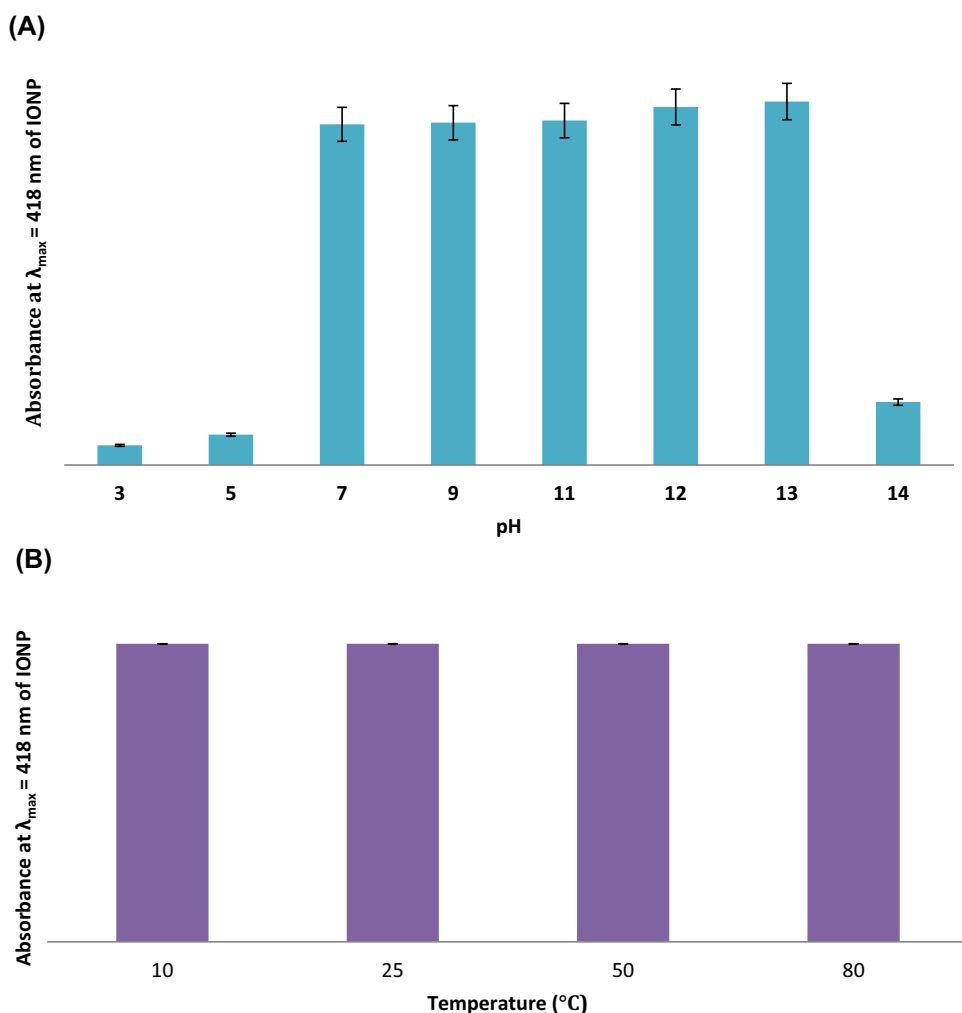
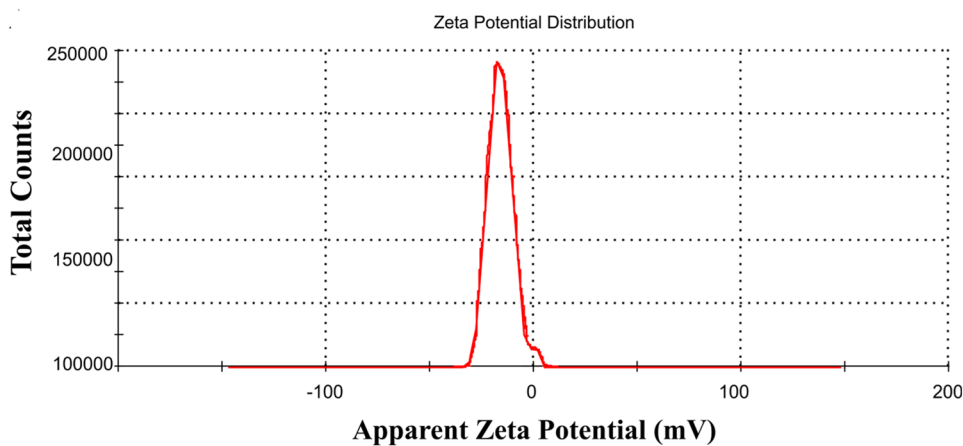


**Fig. 4** Zeta potential of synthesized iron oxide nanoparticle



orisation for Azo violet was attained at 4.5 gm/l; while, for Congo red, the saturation was attained at 5 gm/l. Similar saturation kinetics has been observed in many earlier studies (Tayeb et al. 2019; Ramezani 2013). It is due to the fact that sufficient sites are available at lower dye concentration for adsorption of dye molecules which gets occupied by dye

molecules at higher dye concentrations causing saturation of the further decolorisation process (Kale and Kane 2016).

**IONP Concentration** The concentration of dye (0.1 gm/l) at which the highest percent decolorisation was observed was taken for studying the effect of IONP concentration

on dye decolorisation. The percentage decolorisation was found to decrease with decreasing concentration of IONPs (Table 4). This is in concordance with the fact that the higher the number of nanoparticles, the more is the availability of sites for attacking the chromophoric system of the dye (Parvin et al. 2018). Thus, the highest decolorisation of  $79.88 \pm 0.04\%$  and  $69.27 \pm 0.02\%$ , respectively, was observed at IONP concentration of  $2.4 \times 10^{11}$  particles/ml for both the dyes.

**pH** Increase in pH increases efficacy of azo dye decolorisation. At dye concentration of 0.1 gm/l and IONP concentration of  $2.4 \times 10^{11}$  particles/ml, maximum decolorisation of  $78.98 \pm 0.05\%$  and  $68.98 \pm 0.04\%$  was achieved at pH 10 (Fig. 5). This is due to electrostatic attraction between cationic dyes and anionic nanoparticles (Mortazavi et al. 2016); therefore, alkaline medium increases dye adsorption. However, in contrast, it has also been observed that for both

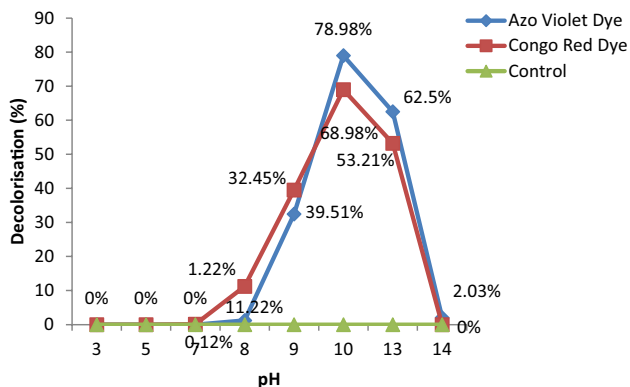


Fig. 5 Effect of pH on dye decolorisation

Table 3 Effect of initial dye concentration on decolorisation

Initial dye concentration (gm/l)	Azo violet Decolorisation (%)	Congo red Decolorisation (%)
0.1	$79.25 \pm 0.01$	$70.25 \pm 0.04$
0.5	$75.22 \pm 0.01$	$45.02 \pm 0.01$
1	$62.08 \pm 0.04$	$32.81 \pm 0.02$
1.5	$57.87 \pm 0.08$	$27.19 \pm 0.04$
2	$38.17 \pm 0.02$	$18.97 \pm 0.05$
2.5	$31.13 \pm 0.03$	$11.93 \pm 0.09$
3	$27.18 \pm 0.02$	$7.54 \pm 0.04$
3.5	$22.17 \pm 0.01$	$2.32 \pm 0.01$
4	$20.83 \pm 0.01$	$1.12 \pm 0.02$
4.5	$17.85 \pm 0.08$	$1.01 \pm 0.04$
5	$11.22 \pm 0.08$	$0.74 \pm 0.02$
10	$2.31 \pm 0.01$	$0.22 \pm 0.01$

Table 4 Effect of IONP concentration on dye decolorisation

IONP concentration (particles/ml)	Azo violet Decolorisation (%)	Congo red Decolorisation (%)
$2.4 \times 10^{11}$	$79.88 \pm 0.04$	$69.27 \pm 0.02$
$2.4 \times 10^{10}$	$11.45 \pm 0.01$	$11.45 \pm 0.07$
$2.4 \times 10^9$	$0.03 \pm 0.01$	$0.03 \pm 0.01$

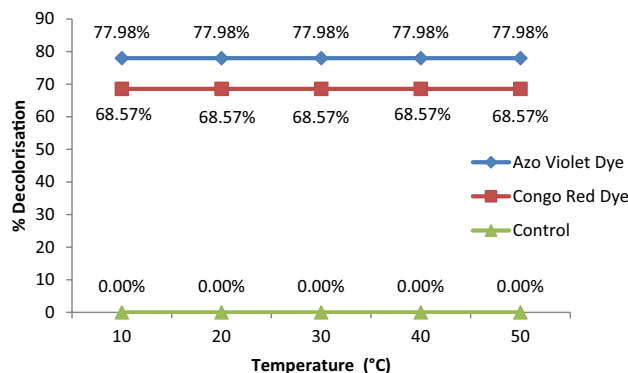


Fig. 6 Effect of temperature on dye decolorisation

the dyes at a pH above 13, the dye adsorption dramatically decreases. This might be associated with destabilization of the synthesized IONPs.

**Temperature** No significant difference in decolorisation has been observed with alteration of temperature (Fig. 6). A constant decolorisation of  $77.98 \pm 0.04\%$  and  $68.57 \pm 0.01\%$  was, respectively, observed for Azo violet and Congo red. This might be correlated to the fact that temperature has no effect on the stability of nanoparticles (as stated in 3.2); thus, altering pH did not alter effect the decolorisation ability of the nanoparticles. However, this is in contrast to the earlier studies that have depicted the effect of temperature on remediation capacity of IONPs (Osman et al. 2015; Sarvari et al. 2018).

**Taguchi Optimization Method (TOM)**

The initial screening experiments depicted that the parameters, viz., initial dye concentration, IONP concentration, and pH, affected the remedial process at its most. These parameters, therefore, were chosen for designing the remediation experiments. Temperature was eliminated from the Taguchi design due to non-significant role as a process parameter. Three most efficient levels for each parameter were chosen (Table 2) in accordance with Taguchi L9 design.

Nine experiments were performed according to the design of experiment as provided by Taguchi design and each

**Table 5** Calculated mean of response and *S/N* ratio for obtained from azo dye decolorisation experiments

Level	Dye concentration	IONP concentration	pH
<i>S/N</i> ratio: azo violet			
1	<b>3.265</b>	– 11.081	– 27.092
2	– 8.075	– 6.589	– 24.316
3	– 15.342	<b>2.482</b>	<b>30.256</b>
Delta	17.607	7.598	57.348
Rank	2	3	1
<i>S/N</i> ratio: Congo red			
1	<b>5.536</b>	– 4.709	– 10.030
2	4.165	2.939	– 11.067
3	– 5.556	<b>5.914</b>	<b>25.241</b>
Delta	11.092	10.623	36.308
Rank	2	3	1

The bold values at each column of this table refer to maximum calculated *S/N* ratio according to the “larger is better” criterion

experiment was repeated thrice, and the results (removal efficiency) were denoted by R1, R2 and R3 (Tables 6, 7).

For both the dyes, the *S/N* ratio plot as shown in Table 5 depicts that increase in initial dye concentration ‘A’ decreases decolorisation efficacy while increasing IONP concentration ‘B’ and pH ‘C’ increases decolorisation efficacy. The maximum value of *S/N* ratio represents optimum level of operational variables. Thus optimum level for each variable is determined by maximum *S/N* value. This is in line with the fact that the desirable and undesirable value for the output response is represented by ‘signal’ to ‘noise’ ratio. Thus, optimization of *S/N* ratio is therefore used to optimize decolorisation parameters of both the dyes. The maximum *S/N* ratio corresponding to maximum removal efficiency of azo violet and Congo red for level ‘1’ is 3.265 and 5.536, respectively, level ‘2’ is 2.482 and 5.914, respectively, and level ‘3’ is 30.256 and 25.241.

The optimum combination for maximum decolorisation of both the azo dyes was found to be A1–B3–C3 corresponding to highest *S/N* ratio of 31.936 for Azo violet and 31.502 for Congo red. Thus, the optimal conditions of decolorisation of both the dyes using the IONPs are 1 gm/l of dye concentration,  $2.4 \times 10^{*11}$  particles/ml, and 13 pH (Tables 6, 7).

Furthermore, the analysis of variance (ANOVA) was done for better comprehension of the relative effect of the aforementioned parameters on removal of dyes from the aqueous solution.

The ANOVA analysis has been used in many earlier studies to determine the relative importance of critical parameters in the optimum combination. Apart from this, a larger *F*-value is indicative of more influence of the parameter on process performance (Madan and Wasewar 2017). The ANOVA analysis in the current case depicts pH as the most influential parameter driving the removal of Azo Violet and Congo Red (Table 8).

Apart from this, percent contribution is another indication for relative ability of parameters. Statistically, factor with a high percent contribution influences the performance even with least variation. It is evident that the factor that highly contributes toward the remediation process of both the dyes is pH with 62% contribution in azo violet remediation and 74% contribution in congo-red remediation. pH is then followed by Initial Dye concentration > IONP concentration for both the dyes (Fig. 7). This indicates that any variation in pH will show prominent difference in the remediation process (Ramezani 2013).

## Kinetics of Dye Decolorisation

### Effect of IONPs’ Concentration on Kinetics of Decolorisation

The decolorisation of dyes by IONPs at most optimal condition is first order with respect to IONP at lower

**Table 6** Design of experiment for azo violet

(A) Dye concentration (gm/l)	(B) IONP concentration (particles/ml)	(C) pH	R1 (%)	R2 (%)	R3 (%)	R (mean) (%)	STDV	<i>S/N</i> ratio
0.1	$2.4 \times 10^{*9}$	11	0.14	0.12	0.11	0.123333	0.015275	– 18.1784
0.1	$2.4 \times 10^{*10}$	12	0.25	0.25	0.26	0.253333	0.005774	– 11.9262
0.1	$2.4 \times 10^{*11}$	13	79.87	79.08	79.98	79.64333	0.490951	36.89907
1	$2.4 \times 10^{*9}$	12	0.08	0.05	0.07	0.066667	0.015275	– 23.5218
<b>1</b>	<b><math>2.4 \times 10^{*11}</math></b>	<b>13</b>	<b>79.98</b>	<b>79.22</b>	<b>79.36</b>	<b>79.52</b>	<b>0.404475</b>	<b>31.93634</b>
1	$2.4 \times 10^{*10}$	11	0.02	0.04	0.01	0.023333	0.015275	– 32.6405
1.5	$2.4 \times 10^{*9}$	13	12.44	12.27	12.77	12.49333	0.254231	21.93357
1.5	$2.4 \times 10^{*10}$	11	0.02	0.02	0.05	0.03	0.017321	– 30.4576
1.5	$2.4 \times 10^{*11}$	12	0.01	0.01	0.02	0.013333	0.005774	– 37.5012

The bold value refer to maximum calculated *S/N* ratio according to the “larger is better” criteria



**Table 7** Design of experiment for Congo red

(A) Dye concentration (gm/l)	(B) IONP concentration (particles/ml)	(C) pH	R1 (%)	R2 (%)	R3 (%)	R (mean) (%)	STDV	S/N ratio
0.1	$2.4 \times 10^9$	11	0.23	0.22	0.22	0.223333	0.005774	- 13.0209
0.1	$2.4 \times 10^{10}$	12	0.51	0.36	0.55	0.473333	0.100167	- 6.49666
0.1	$2.4 \times 10^{11}$	13	65.89	64.28	61.85	64.00667	2.033822	36.1245
1	$2.4 \times 10^9$	12	0.37	0.33	0.34	0.346667	0.020817	- 9.20176
<b>1</b>	<b><math>2.4 \times 10^{11}</math></b>	<b>13</b>	<b>69.3</b>	<b>67.22</b>	<b>66.27</b>	<b>67.59667</b>	<b>1.54972</b>	<b>31.50299</b>
1	$2.4 \times 10^{10}$	11	0.21	0.45	0.31	0.323333	0.120554	- 9.80699
1.5	$2.4 \times 10^9$	13	2.88	2.15	2.59	2.54	0.36756	8.096674
1.5	$2.4 \times 10^{10}$	11	0.41	0.44	0.45	0.433333	0.020817	- 7.26356
0.1	$2.4 \times 10^{11}$	11	0.23	0.22	0.22	0.223333	0.005774	- 13.0209

The bold value refer to maximum calculated S/N ratio according to the "larger is better" criteria

**Table 8** ANOVA for mean response

Operational variable	DOF	SS	MS	F-ratio (F)	P (%)
ANOVA for remediation experiments: azo violet					
Dye concentration	2	557.9	278.9	1.02	0.498
IONP concentration	2	548.3	274.2	1.00	0.500
pH	2	3293.2	1646.6	<b>6.01</b>	0.143
Error	2	548.0	274.0		
Total	8	4947.4			
ANOVA for remediation experiments: Congo red					
Dye concentration	2	636.6	318.3	1.01	0.498
IONP concentration	2	632.3	316.2	1.00	0.500
pH	2	2365.7	1182.8	<b>3.74</b>	2.11
Error	2	632.7	316.4		
Total	8	4267.3			

The bold value refer to maximum calculated S/N ratio according to the "larger is better" criteria

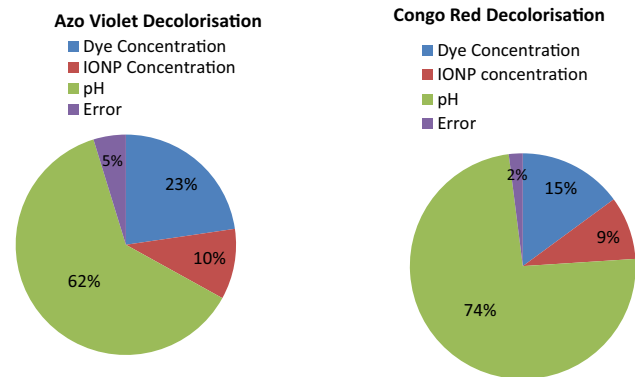


**Fig. 7** Percentage impact of each parameter on the azo dye decolorisation

concentrations. This means when the IONP concentration was low, the decolorisation percentage was low, as well.

However, when the concentration of the nanoparticles (reagent) was increased, the decolorisation rate increased (Fig. 8).

For both the dyes, a raise in concentration from  $2.4 \times 10^9$  particles/ml to  $2.4 \times 10^{10}$  particles/ml doubles the rate of reaction from  $0.6 \times 10^{-2} \text{ min}^{-1}$  to  $1.2 \times 10^{-2} \text{ min}^{-1}$  in case of Azo violet and  $2.4 \times 10^{-2} \text{ min}^{-1}$  to  $4.8 \times 10^{-2} \text{ min}^{-1}$  in case of Congo Red (Table 9). Whereas, the increase in concentration of IONPs further ten times ( $2.4 \times 10^{11}$  particles/ml) did not increase the rate of reaction proportionally. This clearly points toward mixed order kinetics for decolorisation of both the dyes.

**Effect of Agitation on Kinetics**

Agitation did not show any significant alteration in the percent decolorisation of dyes, but it hastened the speed of decolorisation reaction for the azo violet dye. The maximal decolorisation of  $77.3 \pm 0.04\%$  was observed at 1.45 h in shaking conditions, while in static condition, the maximal decolorisation time was 2.55 h (Fig. 9a). While, in case of congo red, shaking conditions did not alter the speed of decolorisation. It was observed that  $70.74 \pm 0.02\%$  of decolorisation was obtained in 4.55 h in both the conditions (Fig. 9b). This is in concordance with the least square regression analysis that depicts that the rate constant (*k*) is lower in static condition ( $1.3 \times 10^{-2} \text{ min}^{-1}$ ) while shaking enhances the rate constant to ( $4.0 \times 10^{-2} \text{ min}^{-1}$ ), thereby proving that in case of azo violet, shaking showcases significant improvement in decolorisation rate without altering the maximal decolorisation ability of the IONPs. Earlier studies have reported similar phenomenon and has associated this with availability of greater number of adsorption sites on the nanoparticle in the initial stage of the reaction; however, as the reaction proceeds, the availability of adsorption sites gets reduced leading to saturation kinetics (Rahman et al. 2015). In such a condition, shaking enhances the rate of reaction

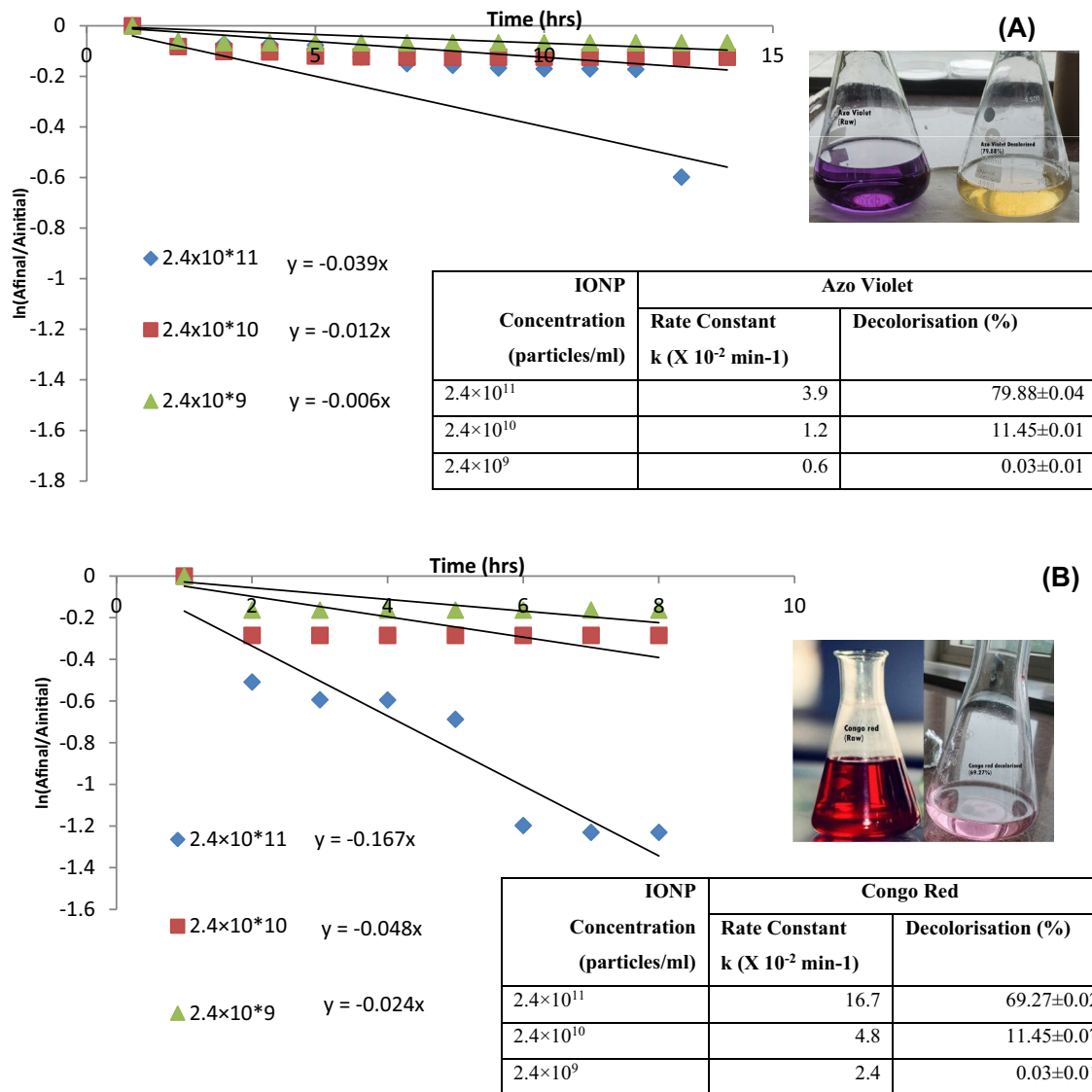


Fig. 8 Effect of IONP concentration on a azo violet decolorisation; b congo-red decolorisation kinetics

Table 9 Efficacy comparison of current decolorisation strategy with earlier literature

Decolorisation method	Decolorisation agent used	Decolorisation efficiency (%)	Decolorisation time (min/l)	References
Coagulation-flocculation	Coagulant derived from <i>Cassia fistula</i>	93.83	60	Dao et al., (2021)
Bio-decolorisation	<i>Pseudomonas putida</i> immobilized in coconut fiber	87	120	Senet al., (2019)
Biological-adsorption	Saw dust, and inorganic soils, such as kaolin	33.5	72	Mirbagheri and Charkhestani (2015)
Phytoremediation	Alligator weed ( <i>A. philoxeroides</i> )	59	96	Rane et al., 2015
<b>Nanoremediation</b>	<b>Bacterial EPS stabilized IONPs</b>	<b>81.40</b>	<b>7.5</b>	<b>Current strategy</b>

The bold value refer to maximum calculated S/N ratio according to the "larger is better" criteria

by increasing the initial kinetic energy of the adsorbent particles as well as the dye molecules (Adeyemo et al. 2015).

However, in case of Congo red, the rate of reaction in case of both shaking and static conditions has no significant

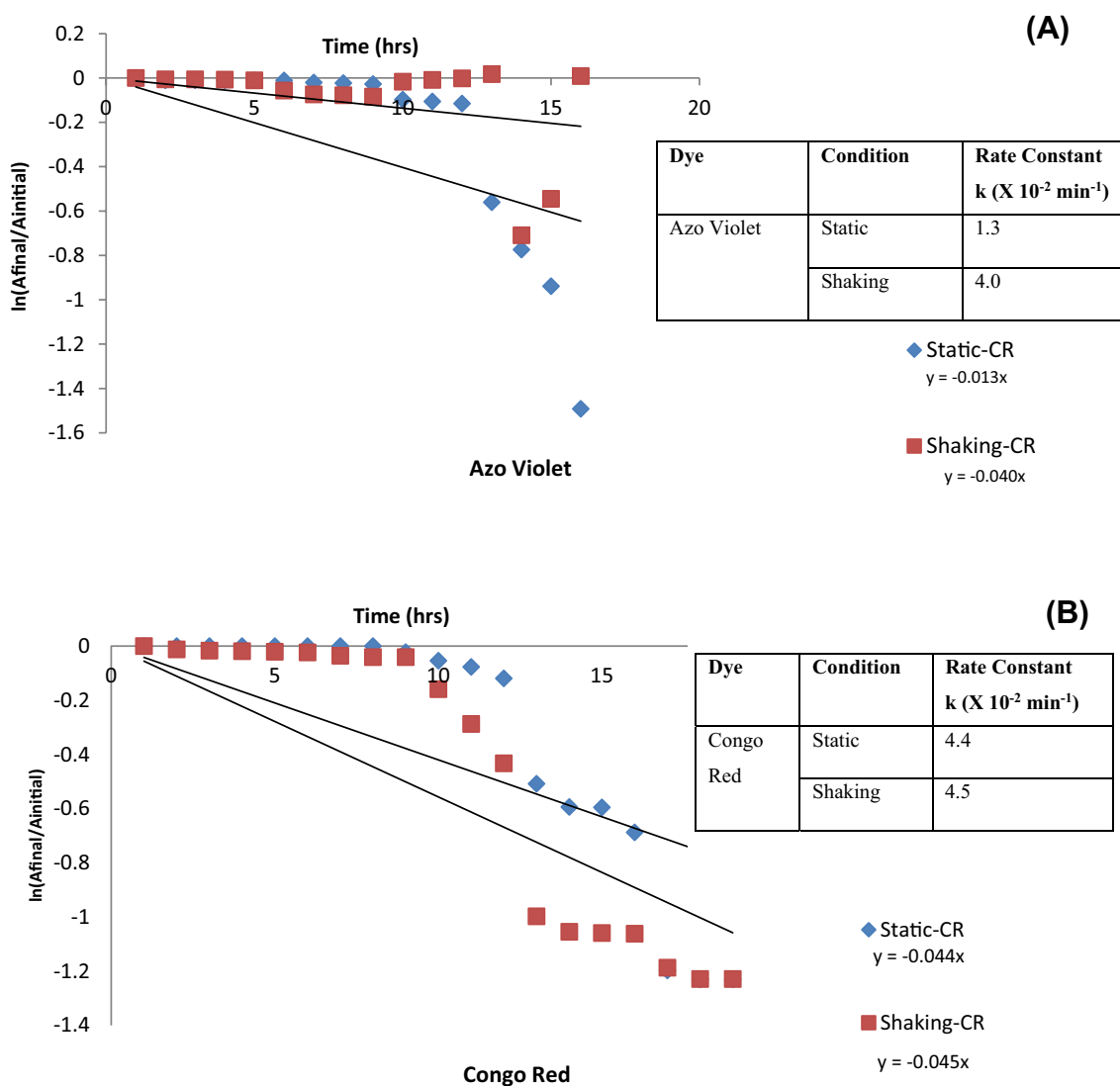


Fig. 9 Effect of agitation on a) azo violet decolorisation; b) congo-red decolorisation kinetics

variation. This might be due to the complexity of the Congo red molecule. Many studies have reported that decolorisation is faster when the dye molecule is less complex with low number of aromatic rings and has small size (Kumar et al. 2012). In this case, the azo violet is smaller with molecular mass (366.71 g/mol) and two aromatic rings as compared to congo red with molecular mass (696.665 g/mol) with structure having six complex aromatic rings (Kumar et al. 2012). Thus, shaking conditions were insufficient in altering reaction rate of the Congo red dye.

### Scale Up to Pilot Scale

In the first phase of the scale-up process, 50 ml of effluent sample was decolorized using 3 ml of IONPs at optimal reaction conditions. Maximal decolorisation of 81.11 ± 0.03%

was attained in 12 min at a rate of 1.35 ml/ml IONP/min (Fig. 10). In the second phase, when the decolorisation process was scaled up to 2.00 l of effluent at optimal condition with constant agitation (150 rpm) in the bioreactor, there was significant enhancement in the rate of reaction without much improvement in percent decolorisation. 15 ml of IONPs were required to reach the maximal decolorisation of 81.40 ± 0.03% in around 15 min, indicating a decolorisation rate of 130 ml/ml IONP/min. Thus, agitation and a constant flow rate of IONPs enhanced the decolorisation rate of dye-rich effluent to 95.29%. The UV-Vis analysis of the effluent depicted the absorbance maxima at 572 nm, which was significantly reduced by the use of IONP (Fig. 10).

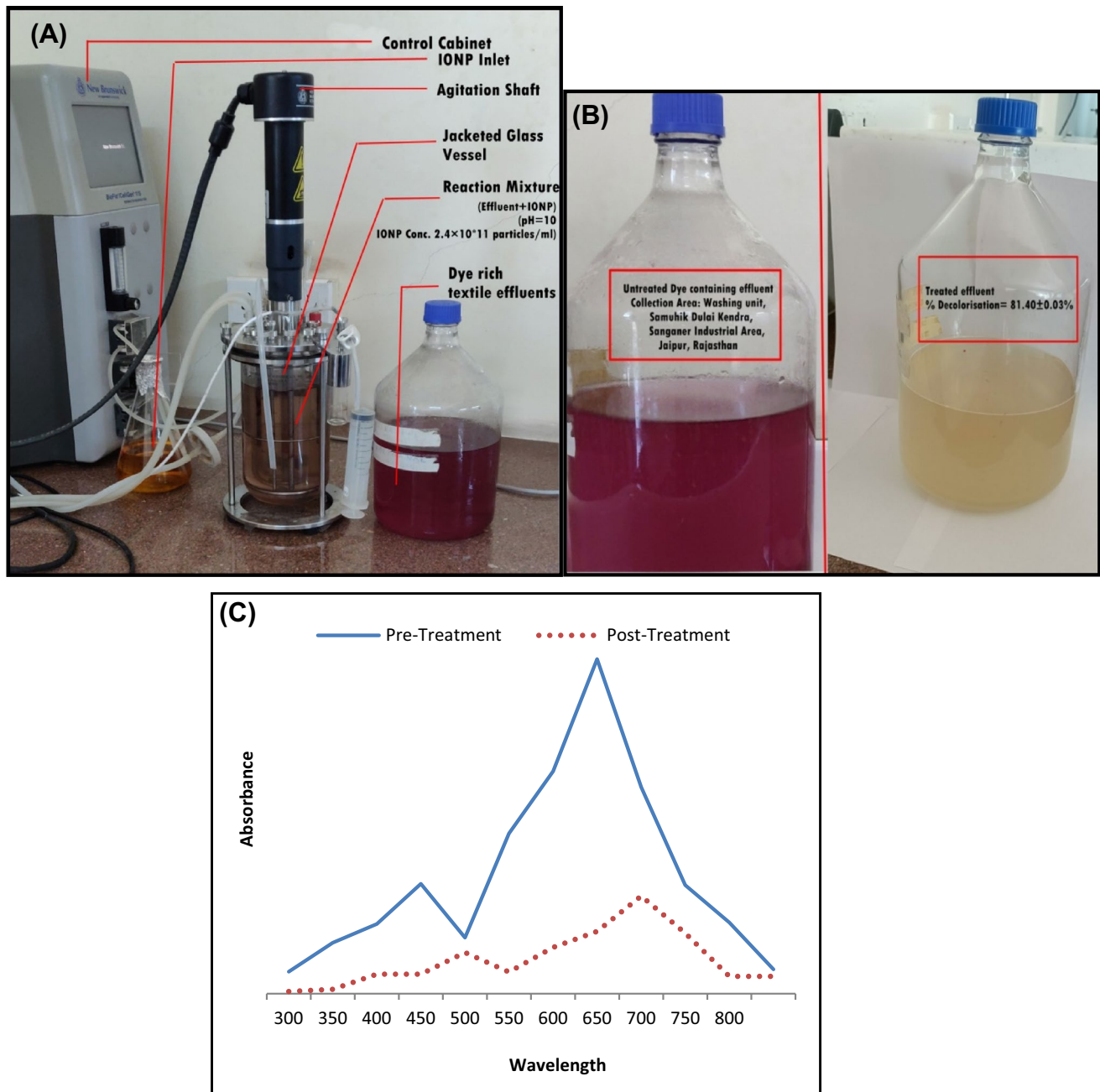


**Fig. 10** **a** Phase II pilot scale remediation setup using New Brunswick BioFlo®/CelliGen® 115 Benchtop Bioreactor. **b** Comparison of untreated and treated effluents from the pilot scale remediation

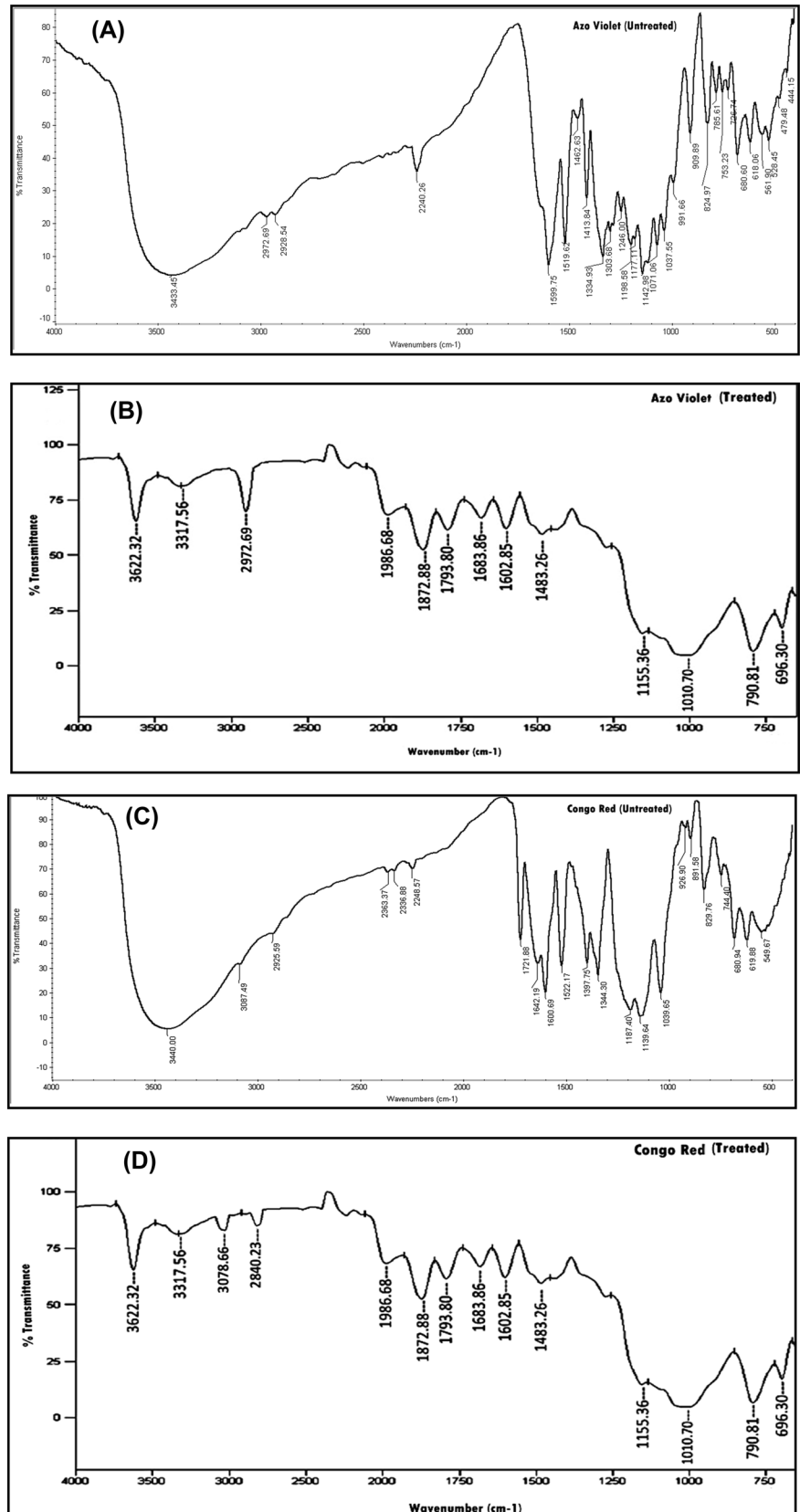
process; **c** UV–Vis spectroscopic analysis of effluent before and after pilot scale remediation process

## Mechanism of Remediation

The comparison of the FTIR spectra with pre- and post-treatment samples of individual dye and the effluent sample clearly depicts removal of the dyes. FTIR spectrum of Azo Violet depicted various bands majorly at 3433, 2972, 1599, 1462, and 785  $\text{cm}^{-1}$  assigned to O–H, –CH aliphatic, C=C, –CH<sub>2</sub> bending, and –C=S, respectively. Similarly, in Congo

red, FTIR depicted major bands at 3440, 2925, 1522, and 829 assigned to O–H, –CH aliphatic, –C=C, and –C=S–, respectively. The FTIR analyses of untreated dye samples show significant alteration when compared to the FTIR spectra of the treated samples (Fig. 11 a–d). FTIR spectrum of the treated samples showed shifts in bands, and appearance and/or disappearance of bands indicating adsorption of the dyes by the IONPs which has led to alteration of

**Fig. 11** FTIR analysis of **a** untreated azo violet sample, **b** treated azo violet sample, **c** untreated congo-red sample, and **d** treated congo-red sample





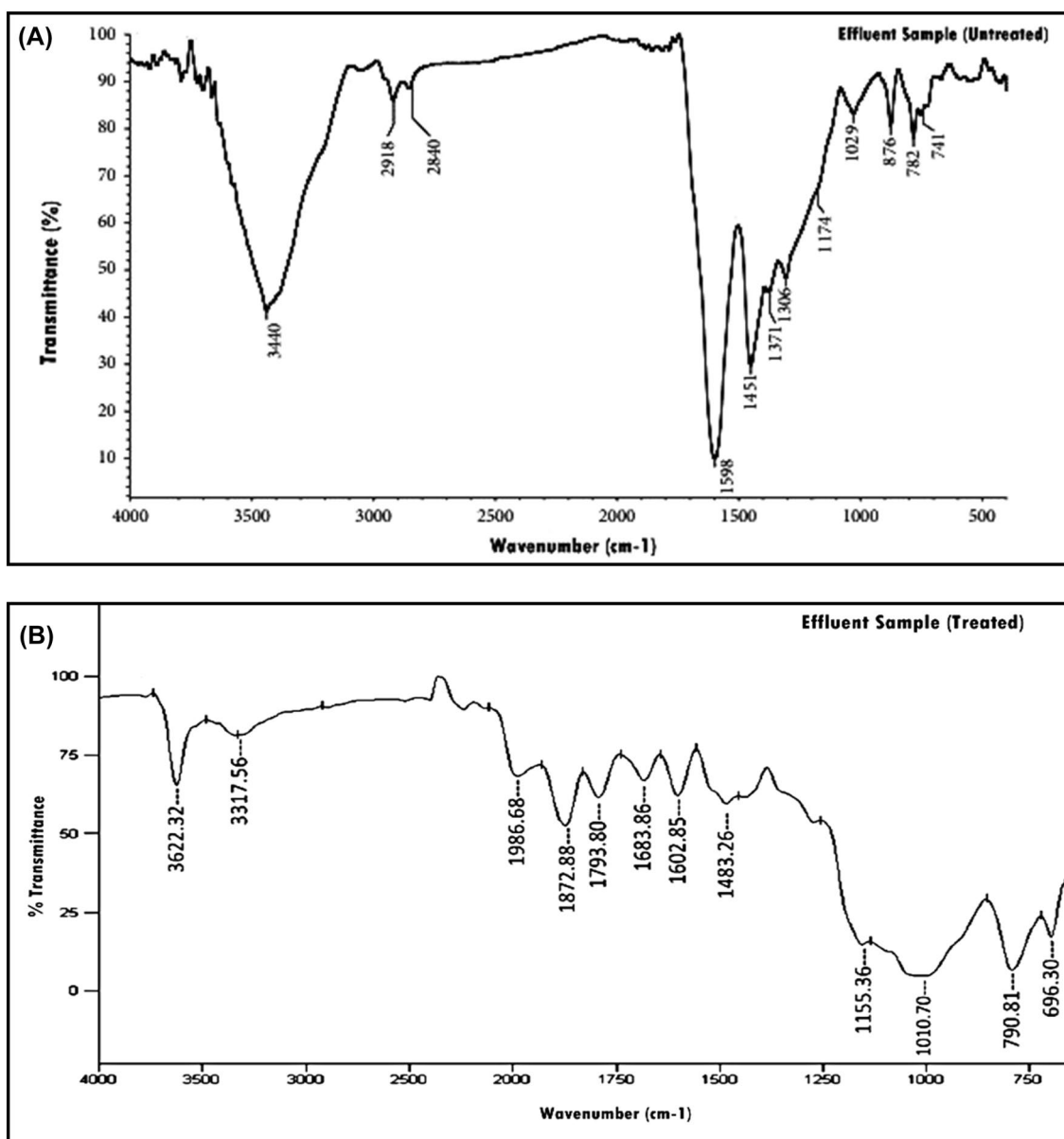


**Fig. 12** FTIR analysis of **a** untreated dye containing effluent sample and **b** treated dye containing effluent sample

functional groups. Such alterations in the post-treated samples are also reported in earlier literature (Abdollahzadeh et al. 2020). The alterations in the FTIR spectra indicate that the interaction of dyes and IONPs in the post-treated samples is mostly driven through hydrogen bonding between the hydroxyl groups of the coagulant and the N-, O-, and/or S-containing groups of the dyes (Fig. 11b, d). Similar variations in FTIR patterns showcasing adsorption of various pollutants using different agents have been reported in earlier studies (Rashtbari et al. 2022; Pourali et al. 2020; Elkady et al. 2020; Dhananasekaran et al. 2016).

Similar variation can also be observed between FTIR peaks of field effluent sample after treatment with IONPs;

thereby indicating adsorption of dyes from the effluent sample by IONPs (Figs. 11, 12).

Furthermore, IONPs harvested from the treated field effluent sample after the pilot scale remediation depicted significant morphological difference when analyzed via HR-TEM (Fig. 13). The micrograph has showed alteration in size of the nanoparticles along with agglomerated morphology. In the treated effluent, the size of the IONPs increases significantly from an average size of  $176.69 \pm 5$  nm (as reported earlier in Sharma et al. 2020) to  $225.21 \pm 3$  nm (Fig. 13C).

The above results are in concordance with earlier studies depicting nanoparticles with reactive surfaces adsorb pollutants, thereby enhancing the agglomeration tendency. This

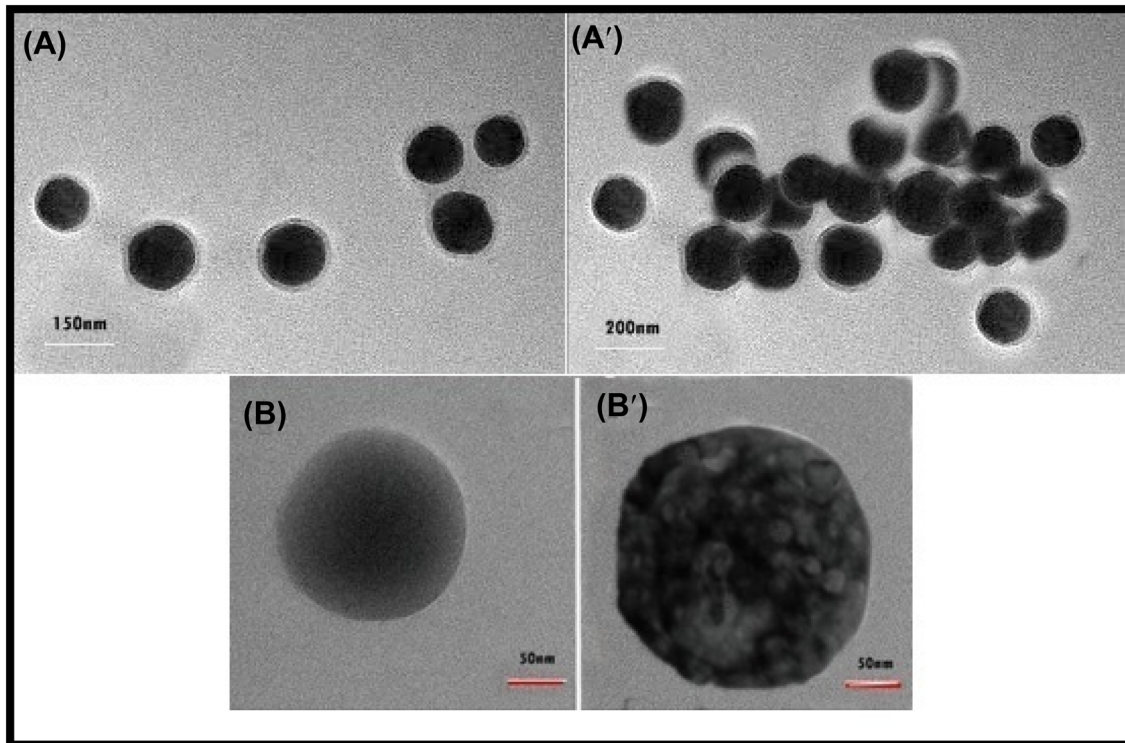


**Fig. 13** **A, B** TEM micrograph of IONPs before treatment of dye containing effluents at different scale bars; **(A', B')** TEM micrograph of IONPs after treatment of dye containing effluents at different scale bars; **C** particle-size distribution of IONPs obtained from TEM analysis

leads to increase in higher mean diameters of the nanoparticles (Önal et al. 2019; Anushree and Philip 2019). Thus, the IONPs are efficient medium to remove azo dyes from waste water as compared to other decolorisation agents. Many methods have been tested on lab scale but few methods that have been tested on field sample through pilot scale. A brief comparison of other pilot tested methods has been presented below to validate working efficacy of the developed IONP-based decolorisation method (Table 9).

Most of the industrially established methods (flocculation, bio-adsorption, etc.) used for decolorisation of dyes have shown good percentage of decolorisation. However, most of the methods require a high retention to achieve the maximal efficiency (as shown in Table 9). This remains the major hurdle in the large-scale treatment. As a huge volume of waste water is being released each hour from a textile dyeing unit, the adaptability of any technology is therefore dependent on its efficiency with respect to its

rapidity (Sharma et al. 2022). Thus, the novelty of the current strategy lies in the fact that, apart from being efficient, the IONPs are quick enough to decolorize huge volumes of textile dye-rich effluents in comparatively lower time. However, some further studies such as immobilization of the IONPs on biodegradable material would further enhance reusability of the decolorizing agent for industrial-level application. Moreover, conducting toxicity studies which would help to identify and derive an eco-friendly scheme for disposability of used nanoparticles would also improve scalability of the process. Furthermore, studies on the process econometrics would help in determining the final scalability of the optimized strategy. The current study will act as a foundation in development of a viable method for establishing Zero Liquid Discharge (ZLD) technologies for effluent treatment in textile industries.

## Conclusion

Knowledge of reaction kinetics is very important to select the suitable reaction design, configuration, and operating conditions for scale-up. In the present study, the IONPs synthesized using  $\text{FeCl}_3 \cdot 6\text{H}_2\text{O}$  and cell-free supernatant of *Alcaligenes* sp. demonstrated stability at alkaline pH (7–13) until 1 year of storage. The immense stability of synthesized nanoparticles makes them amenable. These IONPs demonstrated efficient decolorisation of both the cationic Azo violet ( $79.88 \pm 0.04\%$ ) and Congo red ( $69.27 \pm 0.02\%$ ) dyes. The optimal condition of decolorisation was found to be 1 gm/l of dye concentration,  $2.4 \times 10^{11}$  particles/ml of IONP, and pH 10. The decolorisation reaction proceeds with a rate constant  $3.9 \times 10^{-2} \text{ min}^{-1}$  for Azo violet and  $16.7 \times 10^{-2} \text{ min}^{-1}$  for Congo red with mixed order kinetics. Additionally, the rate of decolorisation for Azo violet was enhanced by constant shaking at 100 r.p.m. without any variation in the maximum decolorisation, while no such variation was observed for Congo red. Many lab-scale studies have been conducted in similar direction, but very few studies have analyzed the efficiency of such nanoparticle based strategies on field samples. The current study therefore has made an attempt to successfully decolorize dye containing effluent collected from washing units of Sanganer Industrial area up to  $81.40 \pm 0.03\%$ . The process when scaled up from 50 ml in static condition to 2 l with agitation has shown a huge increment of rate of decolorisation from 130 ml/ml IONP/min to 1.35 ml/ml IONP/min accounting for rise in rate by 96.29-fold. The variation in the FTIR peaks after the decolorisation process and increased nanoparticle size and its aggregated morphology post-treatment as observed in TEM analysis proved adsorption of the dyes by the IONPs. It can be thus concluded that the

synthesized IONPs and optimized conditions above are suitable for decolorisation of recalcitrant azo dyes owing to both their stability and efficacy. Thus, the practical application of the current work is to develop an effective as well as rapid decolorisation strategy for removal of dyes from point-of-discharge channels in textile industry by replacing the conventional time-consuming decolorisation methods.

**Acknowledgements** The authors gratefully acknowledge the help in imaging of the nanoparticles by Central Instruments Facility, IIT Guwahati, Assam, and Dr. Sidananda Sarma, Technical Officer Grade I, IIT Guwahati, Assam, for TEM analysis. Authors would also like to acknowledge Department of Science and Technology, Government of India, New Delhi for providing FIST grant to Amity Institute of Biotechnology, Amity University, Rajasthan, Jaipur-India.

## Declarations


**Conflict of interest** The authors declare no conflict of interest.

## References

- Abdollahzadeh H, Fazlzadeh M, Afshin S et al (2020) Efficiency of activated carbon prepared from scrap tires magnetized by  $\text{Fe}_3\text{O}_4$  nanoparticles: characterization and its application for removal of reactive Blue19 from Aquatic Solutions. *Int J Environ Anal Chem* 102(8):1–15
- Adeyemo AA, Adeoye IO, Bello OS (2015) Adsorption of dyes using different types of clay: a review. *Appl Water Sci* 7:543–568
- Anouar H, Anouar E, El Hourch A, El Kacemi K (2014) Density functional theory study of Reactive Violet 5R azo dye. *Int J Innov Appl Res* 9(3):1362–1367
- Anushree C, Philip J (2019) Efficient removal of methylene blue dye using cellulose capped  $\text{Fe}_3\text{O}_4$  nanofluids prepared using oxidation-precipitation method. *Colloids Surf A Physicochem Eng Asp* 567:193–204
- Bendell A et al (eds) (1989) Taguchi methods. McGraw-Hill, New York
- Bezza FA, Tichapondwa SM, Chirwa EMN (2020) Synthesis of biosurfactant stabilized silver nanoparticles, characterization and their potential application for bactericidal purposes. *J Hazard Mater* 393:122–319
- Bhattacharjee S (2016) DLS and zeta potential—what they are and what they are not? *J Control Release* 235:337–351
- Chen Q, Gu X, Wang Y, Jing D (2013) Synthesis of nanocrystalline yttrium iron oxides and their activity for photocatalytic hydrogen evolution. *Sci Adv Mater* 5:1117–1122
- Dao MT, Nguyen VCN, Tran TN et al (2021) Pilot-scale study of real domestic textile wastewater treatment using Cassia fistula seed-derived coagulant. *J Chem* 2021:1–8
- Desai C, Jain KR, Boopathy R, Van Hullebusch ED, Madamwar D (2021) Editorial: Eco-sustainable bioremediation of textile dye wastewaters: innovative microbial treatment technologies and mechanistic insights of textile dye biodegradation. *Front Microbiol* 12:707083
- Dhananasekaran S, Palanivel R, Pappu S (2016) Adsorption of methylene blue, bromophenol blue, and Coomassie Brilliant Blue by  $\alpha$ -chitin nanoparticles. *J Adv Res* 7:113–124
- Dutta S, Gupta B, Srivastava SK, Gupta AK (2021) Recent advances on the removal of dyes from wastewater using various adsorbents. *Crit Rev Solid State Mater Sci* 2:4497–4531

- Elkady M, Shokry H, Hamad H (2020) New activated carbon from mine coal for adsorption of dye in simulated water or multiple heavy metals in real wastewater. *Mater* 13:2498
- Ghaly AE, Ananthashankar R, Alhattab M, Ramakrishnan VV (2013) Production, characterization and treatment of textile effluents: a critical review. *Chem Eng Process* 5:1–18
- Hendel T, Wuitschick M, Kettemann F, Birnbaum A, Rademann K, Polte J (2014) In situ determination of colloidal gold concentrations with UV–Vis spectroscopy: limitations and perspectives. *Anal Chem* 86(22):11115–11124
- Holkar CR, Jadhav AJ, Pinjari DV, Mahamuni NM, Pandit AB (2016) A critical review on textile wastewater treatments: possible approaches. *J Environ Manag* 182:351–366
- Kale RD, Kane PB (2016) Colour removal using nanoparticles. *Text Cloth Sustain* 2:4
- Kalliola S, Repo E, Sillanpää M, Arora JS, He J, John VT (2016) The stability of green nanoparticles in increased pH and salinity for applications in oil spill-treatment. *Colloid Surface A* 493:99–107
- Kumar CG, Mongolla P, Joseph J, Sarma VU (2012) Decolorization and biodegradation of triphenylmethane dye, brilliant green, by *Aspergillus* sp. isolated from Ladakh, India. *Process Biochem* 47:1388–1394
- Lázár I, Szabó H (2018) Prevention of the aggregation of nanoparticles during the synthesis of nanogold-containing silica aerogels. *Gels* 4:55
- Ledakowicz S, Paździor K (2021) Recent achievements in dyes removal focused on advanced oxidation processes integrated with biological methods. *MOLEFW* 26:870
- Madan SS, Wasewar KL (2017) Optimization for benzenoacetic acid removal from aqueous solution using CaO<sub>2</sub> nanoparticles based on Taguchi method. *J Appl Res Technol* 15:332–339
- Mirbagheri SA, Charkhestani A (2015) Pilot-scale treatment of textile wastewater by combined biological-adsorption process. *Desalin Water Treat* 57(20):9082–9092
- Mortazavi K, Rajabi H, Ansari A, Ghaedi M, Dashtian K (2016) Preparation of silver nanoparticle loaded on activated carbon and its application for removal of Malachite Green from aqueous solution. *Inorg NanoMet*
- Önal ES, Yatkin T, Aslanov T (2019) Biosynthesis and characterization of iron nanoparticles for effective adsorption of Cr(VI). *Int J Chem Eng* 2019:1–13
- Osman MS, Kong L, Ahmad N, Lim J (2015) Role of temperature and pH on the dye degradation using magnetic nanoparticles augmented polymeric microcapsule. *Adv Mater Res* 1113:566–570
- Parvin F, Nayna OK, Tareq SM et al (2018) Facile synthesis of iron oxide nanoparticle and synergistic effect of iron nanoparticle in the presence of sunlight for the degradation of DOM from textile wastewater. *Appl Water Sci* 8(2):73
- Pourali P, Behzad M, Arfaeinia H et al (2020) Removal of acid blue 113 from aqueous solutions using low-cost adsorbent: adsorption isotherms, thermodynamics, kinetics and regeneration studies. *Sep Sci Technol* 56:3079–3091
- Rafique MA, Kiran S, Javed S et al (2021) Green synthesis of nickel oxide nanoparticles using *Allium cepa* peels for degradation of Congo red direct dye: an environmental remedial approach. *Water Sci Technol* 84:2793–2804
- Rahman AF, Sy Mei L, Abdul JA, Triwahyono S (2015) Photocatalytic decolorization of methylene blue using zinc oxide supported on mesoporous silica nanoparticles. *Malays J Fund Appl Sci* 11(4)
- Ramezani S (2013) Biodegradation of malachite green by *Klebsiella TERRIGENAPTCC 1650*: the critical parameters were optimized using Taguchi optimization method. *J Bioremediat Biodegrad* 04:175
- Rane NR, Chandanshive VV, Watharkar AD et al (2015) Phytoremediation of sulfonated remazol red dye and textile effluents by *Alternanthera philoxeroides*: an anatomical, enzymatic and pilot scale study. *Water Res* 83:271–281
- Rashtbari Y, Américo-Pinheiro JH, Bahrami S et al (2020) Efficiency of zeolite coated with zero-valent iron nanoparticles for removal of humic acid from aqueous solutions. *Water Air Soil Pollut* 231(10):1–15
- Rashtbari Y, Sher F, Afshin S et al (2022) Green synthesis of zero-valent iron nanoparticles and loading effect on activated carbon for Furfural adsorption. *Chemosphere* 287:132114
- Saharan V, Mehrotra A, Khatik R, Rawal P, Sharma SS, Pal A (2013) Synthesis of chitosan based nanoparticles and their in vitro evaluation against phytopathogenic fungi. *Int J Biol Macromol* 62:677–683
- Sarvari H, Goharshadi E, Samiee S, Ashraf N (2018) Removal of Methyl Orange from Aqueous Solutions by Ferromagnetic Fe/Ni Nanoparticles. *Phys Chem Res* 6(2): 433–446
- Sen SK, Patra P, Das CR et al (2019) Pilot-scale evaluation of biodecolorization and biodegradation of reactive textile wastewater: an impact on its use in irrigation of wheat crop. *Water Resour Ind* 21:100106
- Sharma B, Kumari N, Mathur S, Sharma, V (2022) A systematic review on iron-based nanoparticle-mediated clean-up of textile dyes: challenges and prospects of scale-up technologies. *Environ Sci Pollut Res* 29:312–331
- Shao XR, Wei XQ, Song X, Hao LY, Cai XX, Zhang ZR, Peng Q, Lin YF (2015) Independent effect of polymeric nanoparticle zeta potential/surface charge, on their cytotoxicity and affinity to cells. *Cell Prolif* 48(4):465–474
- Sharma B, Menon S, Mathur S, Sharma V (2020) Decolorization of Malachite Green Dye from aqueous solution using biosurfactant-stabilized iron oxide nanoparticles: process optimization and reaction kinetics. *Int J Environ Sci Technol* 18:1739–1752
- Sharma B, Kumari N, Mathur S, Sharma V (2021) A systematic review on iron-based nanoparticle-mediated clean-up of textile dyes: challenges and prospects of scale-up technologies. *Environ Sci Pollut Res* 29:312–331
- Shokoohi R, Samadi MT, Amani M, Poureshgh Y (2018a) Modeling and optimization of removal of cefalexin from aquatic solutions by enzymatic oxidation using experimental design. *Braz J Chem Eng* 35:943–956
- Shokoohi R, TaghiSamadi M, Amani M, Poureshgh Y (2018b) Optimizing laccase-mediated amoxicillin removal by the use of Box–Behnken design in an aqueous solution. *Desalin Water Treat* 119:53–63
- Shrestha S, Wang B, Dutta P (2020) Nanoparticle processing: understanding and controlling aggregation. *Adv Colloid Interface Sci* 279:102162
- Süzen Y, Ozmetin C (2019) Removal of reactive black 5 dye using Fenton oxidation from aqueous solutions and optimization of response surface methodology. *Desalin Water Treat* 172:106–114
- Tahir U, Yasmin A, Khan UH (2016) Phytoremediation: potential flora for synthetic dyestuff metabolism. *J King Saud Univ Sci* 28:119–130
- Tan KB, Vakili M, Horri BA et al (2015) Adsorption of dyes by nanomaterials: recent developments and adsorption mechanisms. *Sep Purif Technol* 150:229–242
- Tayeb AM, Tony MA, Ismaeel EK (2019) Engineered nanostructured ZnO for water remediation: operational parameters effect, Box–Behnken design optimization and kinetic determinations. *Appl Water Sci* 9:43
- Wardani RK, Dahlan K, Wahyudi ST, Sukaryo SG (2019) Synthesis and characterization of nanoparticle magnetite for biomedical application. *AIP Conf Proc* 2914(1)
- Yaseen DA, Scholz M (2018) Textile dye wastewater characteristics and constituents of synthetic effluents: a critical review. *Int J Environ Sci Technol* 16:1193–1226

## Authors and Affiliations

Baby Sharma<sup>1</sup> · Nilima Kumari<sup>2</sup> · Shruti Mathur<sup>1</sup> · Vinay Sharma<sup>1</sup> 

✉ Shruti Mathur  
smathur1@jpr.amity.edu

✉ Vinay Sharma  
vsharma4@jpr.amity.edu; vinaysharma30@yahoo.co.uk

Baby Sharma  
baby.sharma@student.amity.edu

Nilima Kumari  
nilima\_km@yahoo.com

<sup>1</sup> Amity Institute of Biotechnology, Amity University  
Rajasthan, SP-1 Kant Kalwar, NH11C, RIICO Industrial  
Area, Jaipur, Rajasthan 303007, India

<sup>2</sup> Department of Bioscience and Biotechnology, Banasthali  
Vidyapith, Tonk, Rajasthan 304022, India